Electronic Supplementary Information

Bisymmetric coherent acoustic tweezers based on modulation of surface acoustic waves for dynamic and reconfigurable cluster manipulation of particles and cells

Hemin Pan,[a] Deqing Mei,[a] Chengyao Xu,[b] Shuo Han[b] and Yancheng Wang[*a]

[a.]*State Key Laboratory of Fluid Power and Mechatronic Systems, School of Mechanical Engineering, Zhejiang University, Hangzhou 310027, China.*

[b.]*Key Laboratory of Advanced Manufacturing Technology of Zhejiang Province, School of Mechanical Engineering, Zhejiang University, Hangzhou 310027, China*

Corresponding author: Yancheng Wang
E-mail: yanchwang@zju.edu.cn; Tel.: (+86) 571-87951906; Fax: (+86) 571-87951145

Supplementary Materials

The PDF file includes:

Fig. S1 to S6

Note S1 to S3

Table S1

Legends for Movies S1 to S9

References

Other Supplementary Materials for this manuscript include the following:

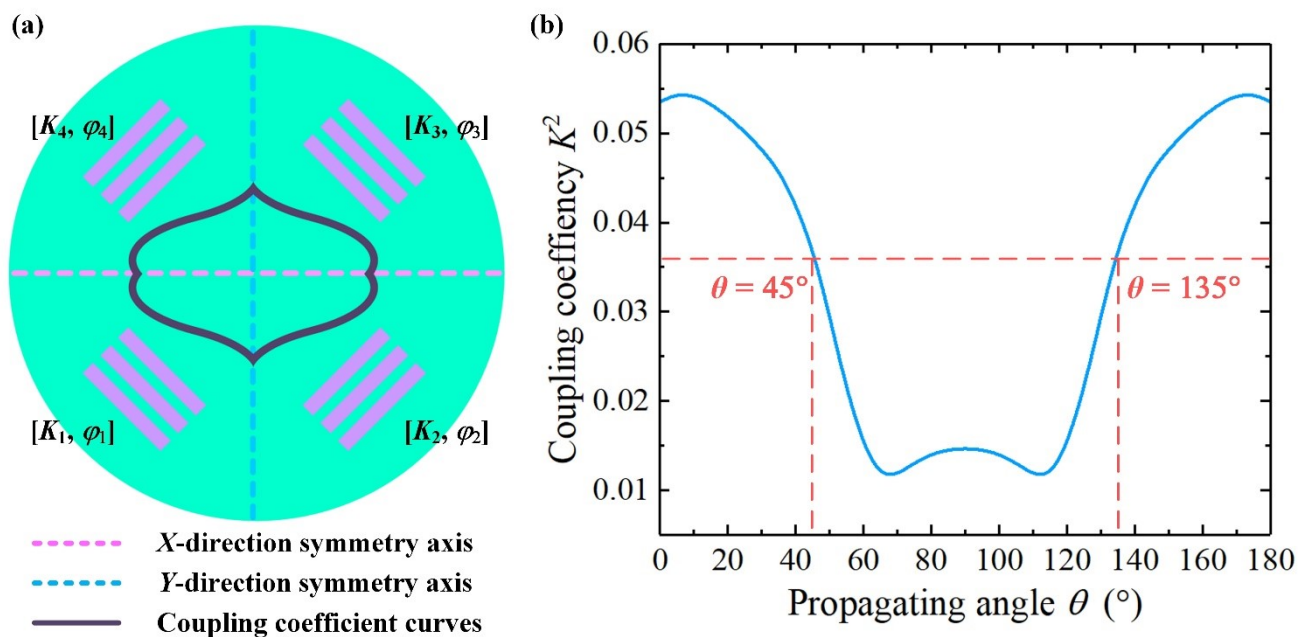Movies S1 to S9

Supplementary Figures.

(a)

(b)

Fig. S1 The dependency of the anisotropic propagation of surface acoustic waves (SAWs) on the 128° Y-cut LiNbO$_3$ substrate. (a) The schematic diagram of IDTs with the bisymmetric arrangement. (b) Calculated electromechanical coupling coefficient (K^2) of the 128° Y-cut LiNbO$_3$ substrate.

Note S1: The four IDTs were set along the two electromechanical coupling coefficient curves symmetric axes of 128° Y-cut LiNbO$_3$ substrate to ensure the intensities of coherent SAWs are identical and sufficient for SAWs generation under the same excitation conditions. And analytical model with governing equations for SAWs propagation was used to determine the electromechanical coupling coefficient (K^2) along any direction on the 128° Y-cut LiNbO$_3$ substrate.[S1, S2]
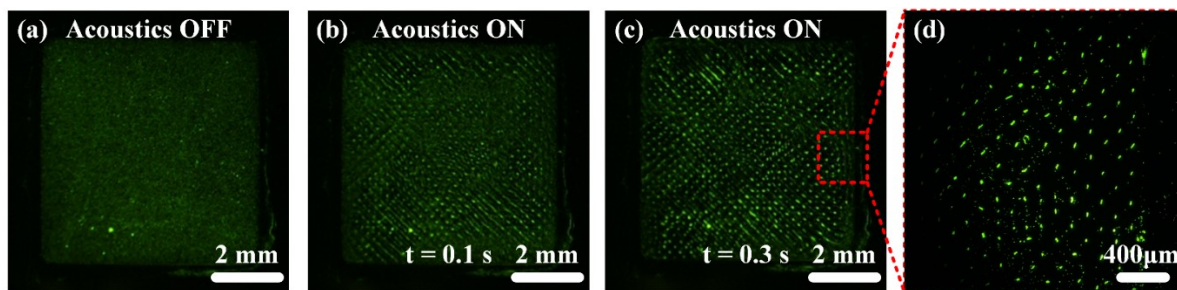

Fig. S2 Real-time patterning of 5 μm PS particles throughout the PDMS chamber. (a) IDTs are turned off and 5 μm PS particles are uniformly distributed within the chamber. (b) After the IDTs are turned on for 0.1 s, the 5 μm PS particles begin to form an array within the chamber. (c) After the IDTs are turned on for 0.3 s, the 5 μm PS particles form a stable array within the chamber. (d) Local zoomed-in view of the stable array.
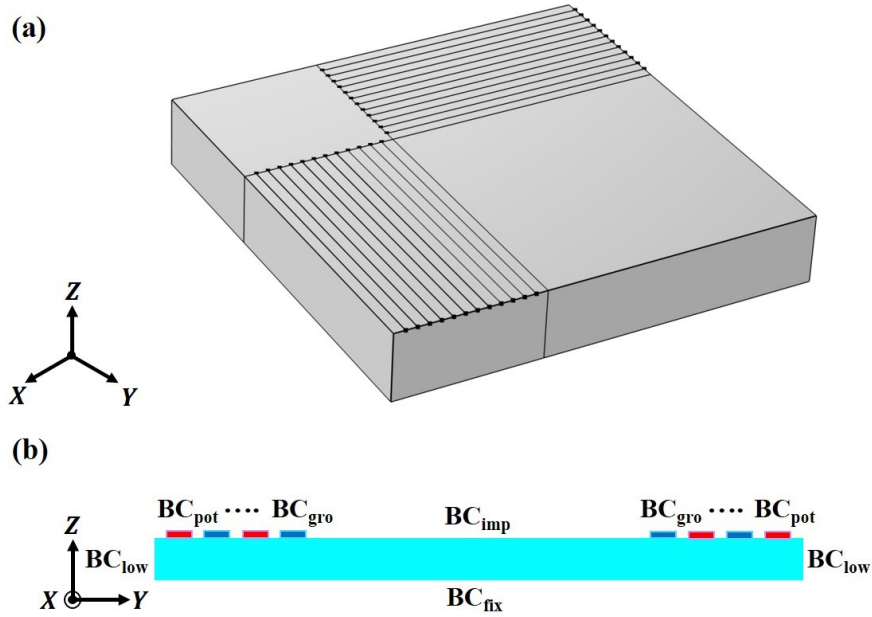
Fig. S3 The diagram of the developed numerical model and boundary conditions set. (a) The established numerical model includes a LiNbO$_3$ substrate layer and four IDTs layers. (b) Schematic diagram of the setting for boundary conditions of the numerical model.

Note S2: Fig. S2b demonstrates the boundary conditions for the established 3D numerical model. A fixed constraint boundary (BC$_{fix}$) is added at the bottom of the 128° Y-cut LiNbO$_3$ substrate layer. Then the boundary conditions of ground (BC$_{gro}$) and electric potential (BC$_{pot}$) are added to the IDTs alternately. The side edges of the LiNbO$_3$ substrate are set as low-reflection boundaries (BC$_{low}$). Finally, the surface of the LiNbO$_3$ substrate layer is set as an impedance boundary (BC$_{imp}$) to simulate the water-filled chamber.
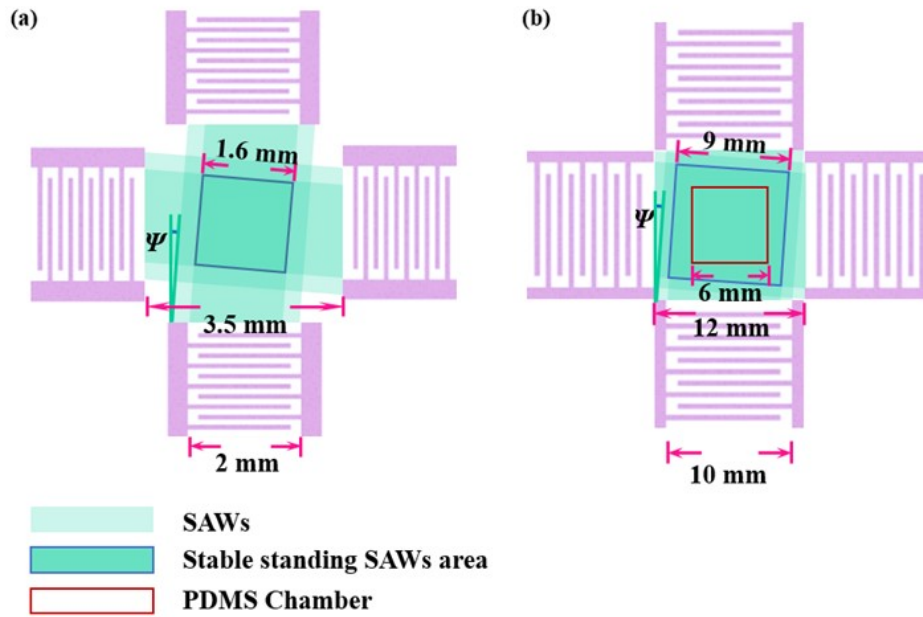
Fig. S4 Effect of power flow angle on the generated stable standing wave area. (a) Predicted stable standing SAWs area with acoustic aperture w = 2 mm and distance between IDTs d = 3.5 mm. (b) Predicted stable standing SAWs area with acoustic aperture w = 10 mm and distance between IDTs d = 12 mm.
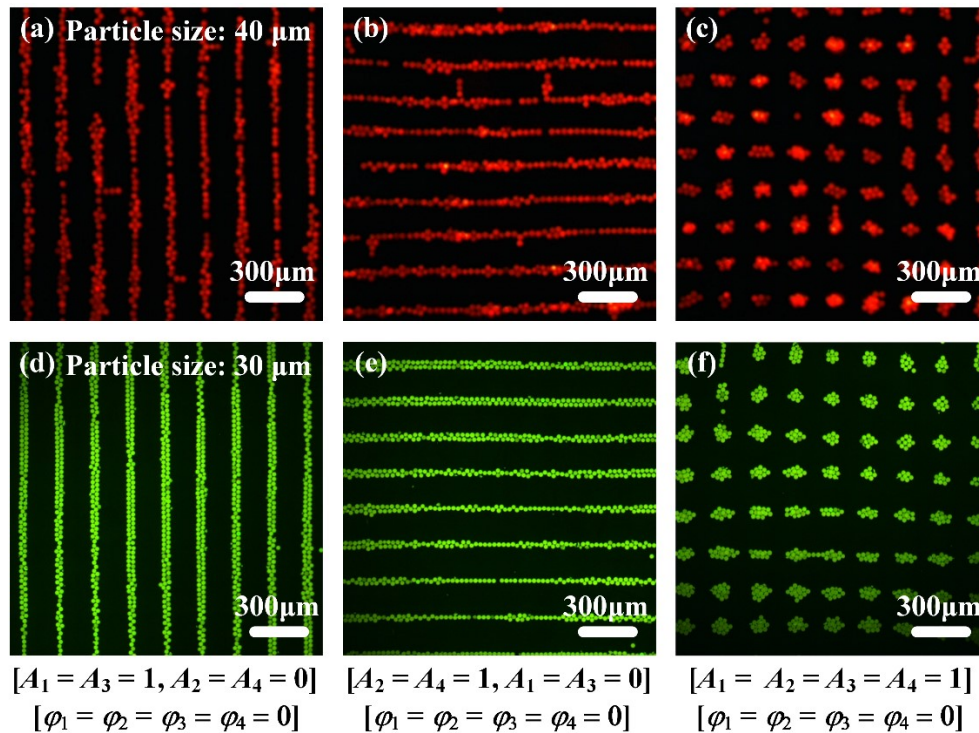

$[A_1 = A_3 = 1, A_2 = A_4 = 0]$ $[A_2 = A_4 = 1, A_1 = A_3 = 0]$ $[A_1 = A_2 = A_3 = A_4 = 1]$
$[\varphi_1 = \varphi_2 = \varphi_3 = \varphi_4 = 0]$ $[\varphi_1 = \varphi_2 = \varphi_3 = \varphi_4 = 0]$ $[\varphi_1 = \varphi_2 = \varphi_3 = \varphi_4 = 0]$

Fig. S5 The patterning arrays of particles with different sizes of the same mass. (a) The vertical stripe array formed by 40 μm PS particles. (b) The horizontal stripe array formed by 40 μm PS particles. (c) The dot array formed by 40 μm PS particles. (d) The vertical stripe array formed by 30 μm magnetic core PS particles. (e) The horizontal stripe array formed by 30 μm magnetic core PS particles. (f) The dot array formed by 30 μm magnetic core PS particles.

Note S3: The density of the 40 μm PS particles we use is 1.07 g/cm3. In contrast, the density of commercially available magnetic core PS particles is 2.31 g/cm3, the diameter of magnetic core PS particle with the same mass as 40 μm PS particle is about 30.9 μm. Therefore, we finally used 30 μm magnetic core PS particles to verify the performance of particle patterning with different sizes of the same mass, as shown in Fig. S4. Based on the same configuration as 40 μm PS particles patterning, the acoustic tweezers manipulated 30 μm magnetic core PS particles to form vertical stripe, horizontal stripe, and dot arrays, respectively. From the experimental results, the 30 μm magnetic core PS particles are significantly better patterned than the 40 μm PS particles with the same particle mass. The above experiment demonstrated that the patterning manipulation of particles is mainly affected by the particle size, where the larger particles will be subject to a larger secondary acoustic radiation force in the acoustic pressure field, leading to the interference with the particle patterning performance.
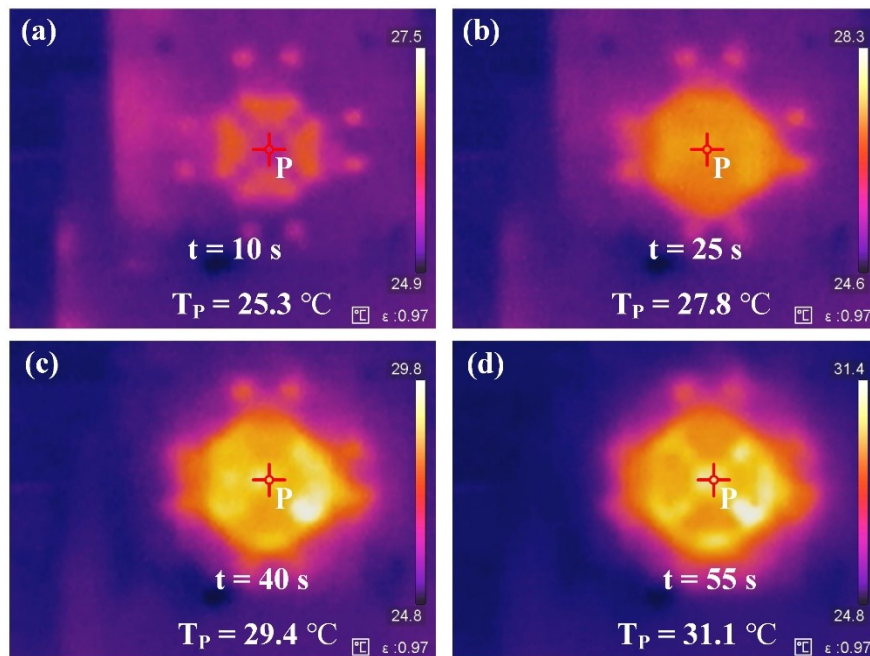

Fig.S6 The infrared holographic temperature distribution of acoustic tweezers over time (a) t = 10s, (b) t = 25s, (c) t = 40s, and (d) t = 55s.

Table S1: The detailed parameters for numerical simulation

Parameter	Value
Density of LiNbO$_3$ substrate	4700 kg/m^3
Speed of acoustic waves (LiNbO$_3$)	3580 m/s
Wavelength	400 μm
Excitation frequency	8.95 MHz
Acoustic impedance	1.497×10^6 Pa·s/m

Supplementary Movies.

Movie S1. Cluster manipulation of 2μm PS particle through coherent SAWs modulation.

Movie S2. Cluster manipulation of 40μm PS particle through coherent SAWs modulation.

Movie S3. Dynamic and reconfigurable manipulation of 2μm PS particle arrays.

Movie S4. Dynamic and reconfigurable manipulation of 40μm PS particle arrays.

Movie S5. Cluster manipulation of yeast cells through coherent SAWs modulation.

Movie S6. Dynamic and reconfigurable manipulation of yeast cell arrays.

Movie S7. Free diffusion and repatterning of yeast cell arrays.

Movie S8. Precise modulation of the geometric parameters of the yeast cell array units.

Movie S9. Controllable translation of the yeast cell array.

Reference

S1.K. Shibayama, K. Yamanouchi, H. Sato and T. Meguro, *Proc. IEEE*, 1976, **64**, 595-597.

S2.S. Sanna and W. G. Schmidt, *Phys. Rev. B*, 2010, **81**, 214116.